Photofragmentation dynamics of the $(N_2O)_2^+$ and $(N_2O)_3^+$ clusters: fragment N_2O^+ A ← X spectra [1]

Sergey A. Nizkorodov [a], Evan J. Bieske [b,*]

[a] *Joint Institute for Laboratory Astrophysics, University of Colorado, Boulder, CO 80309, USA*
[b] *School of Chemistry, The University of Melbourne, Parkville, Vic. 3052, Australia*

Abstract

Rovibrational distributions of N_2O^+ fragments resulting from the direct 640 nm photodissociation of mass-selected $(N_2O)_2^+$ and $(N_2O)_3^+$ clusters have been measured in a tandem mass spectrometer apparatus, via the $A\,^2\Sigma^+ \leftarrow X\,^2\Pi$ predissociative transition of N_2O^+. The N_2O^+ fragments from the dimer are endowed with significant amounts of rotational energy ($45.5 < J < 85.5$) with both $^2\Pi_{3/2}$ and $^2\Pi_{1/2}$ spin–orbit substrates equally populated. While most of the fragments are formed in the ground vibrational state, a significant fraction have a single quantum of ν_1 (1126 cm^{-1}) or ν_3 (1737 cm^{-1}) or several quanta of ν_2 (457 cm^{-1}). The N_2O^+ fragments from the trimer possess significantly less rotational energy than those from the dimer but again a significant fraction is found to be vibrationally excited. The markedly reduced rotational energy of N_2O^+ fragments from the trimer compared to the dimer is consistent with charge and energy transfer processes occurring between the recoiling cluster subunits. © 1998 Elsevier Science B.V. All rights reserved.

1. Introduction

Although ionic complexes and clusters are ubiquitous components of ionized gaseous media, many details of their structure and photophysical behaviour remain poorly understood. A case in point concerns the photodynamics of cation homodimers. For species like Ar_2^+, $(N_2)_2^+$, and $(N_2O)_2^+$ exposure to light in the visible or near UV generally leads to direct dissociation on a repulsive surface generating electronic ground state fragments. By measuring the wavelength dependence of the photofragmentation cross-section, and the fragments' spatial and translational kinetic energy distributions, general features of the participating electronic states (symmetries, structures) and energy disposal mechanisms (fragment vibrational, rotational and electronic energy content) have been inferred [1,2]. Despite the ability of mass spectroscopically based kinetic energy release experiments to provide a broad picture of the photoinduced breakup of ionic homodimers, specific details of the energy partitioning accompanying photodecomposition remain obscure, particularly regarding the proportioning of energy between the fragments' rotational and vibrational degrees of freedom. Without fragment translational energy measurement with a precision comparable to the fragment vibrational

---

* Corresponding author. Fax: +61-3-9347-5180.
[1] This work was carried out at the Institut für Physikalische Chemie, Universität Basel, Klingelbergstrasse 80, CH-4056, Switzerland.

and rotational level spacings it is difficult to precisely deduce the fragments' fate.

In the current study we have combined mass spectrometric and laser spectroscopic means to explore the rovibrational status of N_2O^+ photofragments ejected from $(N_2O)_n^+$ $(n = 2, 3)$ complexes. The method exploits the fact that the higher vibrational levels of the N_2O^+ $A^2\Sigma^+$ state are predissociative and result in the formation of NO^+ photoproducts. By measuring the NO^+ yield as the probe laser wavelength is scanned it is possible to record a spectrum of nascent N_2O^+ photofragments from mass-selected $(N_2O)_n^+$ $(n = 2, 3)$ complexes [3–5]. A significant feature of the experimental scheme is that the entire procedure is mass selective, eliminating ambiguity in the identities of both parent or product ions. Thus, we are certain that the N_2O^+ fragments which are probed result from the photolysis of a particular sized parent complex. To our knowledge this is the first occasion that the rovibrational status of photofragments from mass-selected ionic complexes has been experimentally assessed. The experimental method is distinguished by high sensitivity and selectivity and can be applied to other complexes containing either N_2O^+ or other ions with well-characterized predissociation behavior.

From high-pressure mass spectrometric and photoionization studies the $(N_2O)_2^+$ dimer is known to be bound by ~ 6100 cm^{-1} with respect to dissociation into ground state N_2O^+ and N_2O fragments [6]. Ab initio calculations [7] indicate that the equilibrium configuration of the dimer has C_{2h} symmetry (as shown in Fig. 1). The coalescence of $^2\Pi$ N_2O^+ and $^1\Sigma^+$ N_2O in C_{2h} symmetry leads to four electronic states A_g, A_u, B_g and B_u, two each correlat-
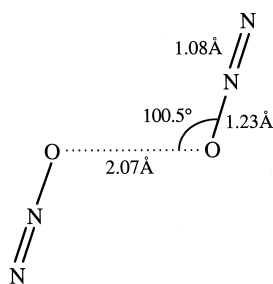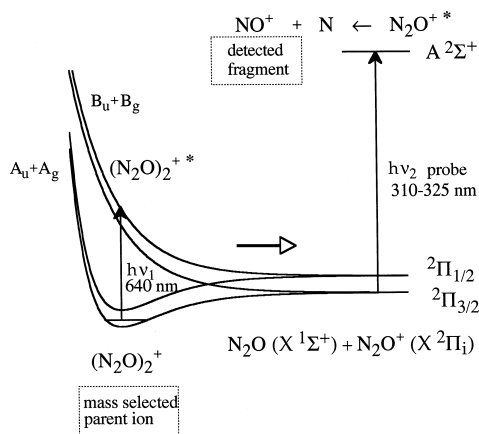

Fig. 2. Experimental scheme for the two-colour pump–probe experiments. The pump laser ($h\nu_1$) excites a transition of mass-selected $(N_2O)_2^+$ cluster ions to the repulsive state. The second laser pulse ($h\nu_2$) probes the rovibrational status of the nascent N_2O^+ photofragments via the $A^2\Sigma^+ \leftarrow X^2\Pi$ predissociative transition of N_2O^+. The spectrum of the fragment N_2O^+ is recorded by measuring the NO^+ signal as a function of ν_2. The setup for assessing the rovibrational status of the N_2O^+ fragments from $(N_2O)_3^+$ cluster ions is similar. As the relevant N_2O^+ $A^2\Sigma^+ \leftarrow X^2\Pi$ absorptions lies at approximately twice the frequency of the $(N_2O)_2^+$ dissociation maximum, the probe beam is generated by doubling the photolysis beam in a KDP crystal. The small change in the photolysis wavelength as the probe frequency is scanned is unlikely to greatly affect the fragmentation dynamics as a directly repulsive surface is accessed.

ing with the upper and lower spin–orbit state of N_2O^+ (separated by ~ 133 cm^{-1}). States having A symmetry are expected to be associated with bound molecular states, while those with B symmetry are repulsive. A reduced dimension representation of the relevant potentials is shown in Fig. 2.

It is apparent from previous work on the $(N_2O)_2^+$ dimer [2] where the translational energy and angular distribution of the N_2O^+ photofragments have been measured, that in the 458–660 nm range photodissociation is direct, ensuing in less than one rotational period with only $\sim 26\%$ of the available energy appearing in fragment translational kinetic energy. Although the whereabouts of the remainder of the available energy was not directly probed in these experiments, it was noted that the translational energy fraction was consistent with an impulsive model with a proportion of the available energy flowing into fragment vibrational degrees of freedom via direct, impulsive interaction between the separating

Fig. 1. Minimum energy C_{2h} structure of the $(N_2O)_2^+$ dimer according to the calculations described in Ref. [7].

N_2O and N_2O^+ moieties. One might expect that if dissociation is mediated through atom–atom repulsions with a starting configuration as shown in Fig. 1, that the fragments should be rotationally excited and may also be endowed with quanta of the bending vibration.

In conjunction with the dimer studies, the photophysical behaviours of the $(N_2O)_3^+$ trimer and the $(N_2O)_4^+$ tetramer have also been assessed, with measurements of photoproduct branching ratios for formation of $(N_2O)_2^+$ and N_2O^+, wavelength-dependent photodissociation cross-sections, and for $(N_2O)_3^+$ measurement of the rovibrational status of the N_2O^+ photofragments. Several questions arise concerning the break-up of the larger $(N_2O)_n^+$ clusters. If the destruction of these species involves a primary absorption by a dimer core, should the resulting N_2O^+ photofragments have a similar rovibrational distribution as N_2O^+ fragments coming from the naked dimer, or are secondary intracluster energy and charge transfer processes also important? Such vibrational and charge transfer appear to play a key role in the photofragmentation of $(N_2)_n^+$ clusters [8,9], with the vibrational energy content of fragment N_2^+ molecules decreasing as the cluster size increases. This result has been explained as due to the exchange of charge and vibrational energy from the nascent N_2^+ resulting from the photolysis of the N_4^+ core with other N_2 ligands as the cluster explodes. The data presented here demonstrate that the proportioning of energy between the N_2O^+ fragment vibration and rotation depends sensitively upon the parent cluster size, suggesting that charge and vibrational energy transfer processes can play an important part in $(N_2O)_n^+$ cluster fragmentation.

2. Experiment

The experiments were performed in quadrupole–octopole–quadrupole tandem mass spectrometer apparatus. As a rather complete description of the apparatus is available in the literature [10], only essential details are provided here. Cluster ions $(N_2O)_n^+$ were produced in a supersonic expansion of pure N_2O (stagnation pressure 4–5 bar) crossed by 200 eV electrons near the nozzle orifice. Fig. 3 shows a mass spectrum taken under these experimental conditions. For the photodissociation cross-sec-
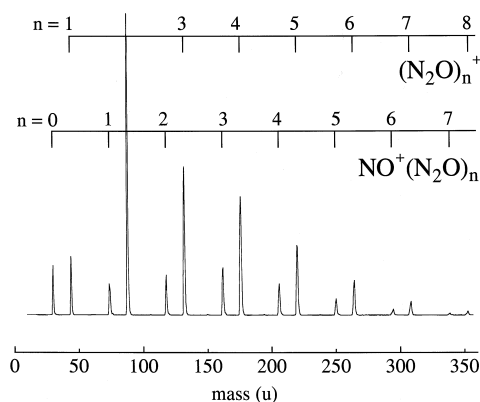

Fig. 3. Typical cluster ion distribution generated by the electron impact ion source for a pure N_2O expansion. The mass spectrum is dominated by the $(N_2O)_n^+$ and the $NO^+(N_2O)_n$ series.

tion and branching ratio measurements, parent clusters were mass selected using the first quadrupole, and were irradiated by the output of a pulsed dye-laser in the octopole ion guide. Photofragments were separated from the parent complexes in a second quadrupole mass filter and assayed by a Daly detector connected either to a photon counter (photodissociation cross-section measurements) or a boxcar integrator (pump–probe experiments). Mass discrimination and transmission loss in the second quadrupole were minimized by reducing its resolution. The pressure in the octopole region was maintained at $\sim 2 \times 10^{-7}$ Torr during the course of the experiment.

Relative photofragmentation cross-sections for the dimer, trimer and tetramer were determined by measuring the ionic photofragment yield as a function of laser power, with the relative cross-section being inferred from the slope of the power-photoyield plot in the linear region. A laser-on/laser-off scheme was adopted to account for fluctuations in the parent ion current and to compensate for collision induced and metastable fragmentation processes. With irradiation, the increase in product ion count equalled the decrease in the parent count within the experimental uncertainty, implying practically complete fragment ion collection. In an attempt to provide an absolute scale for the $(N_2O)_n^+$ photodissociation cross-sections, a parallel series of measurements with identical laser alignment, lens settings, ion beam energy, and source conditions, were conducted on Ar_3^+ for

which wavelength-dependent total photodestruction cross-sections have been reported [1,11]. It is relevant to note that the form of the Ar_3^+ absorption profile and its absolute scale may depend somewhat upon the ions' internal energy. While this may affect the absolute values of the cross-sections reported here, the relative cross-sections for $(N_2O)_n^+$ ($n = 2–4$) photofragmentation at each wavelength should still be correct. The $(N_2O)_3^+$ trimer and $(N_2O)_4^+$ tetramer were observed to photofragment into both N_2O^+ and $(N_2O)_2^+$ cation products, with the branching ratio depending upon the laser wavelength, shorter wavelengths promoting more extensive fragmentation.

The rovibrational status of N_2O^+ cations ejected from the photolysed $(N_2O)_n^+$ complexes was investigated in a two-laser, pump–probe experiment (Fig. 2). A visible photolysis laser pulse excites a dissociative transition in the $(N_2O)_n^+$ ($n = 2, 3$) complex as they pass through the octopole, leading to ejection of N_2O^+ and N_2O neutral(s). A second tunable laser pulse in the near UV probes the nascent N_2O^+ fragments by exciting the $A\,^2\Sigma^+ \leftarrow X\,^2\Pi$ predissociative transition to give NO^+ fragments that are subsequently transmitted by the second quadrupole and detected. A rather simple laser setup is possible for the photolysis/probe experiments, as the relevant N_2O^+ $A\,^2\Sigma^+ \leftarrow X\,^2\Pi$ absorptions lies at approximately twice the frequency of the $(N_2O)_2^+$ dissociation maximum. Thus, the photolysis (dye) laser beam is doubled in a KDP crystal in order to produce the necessary probe laser pulse. The polarization of this probe laser pulse is perpendicular to that of the photolysis laser. Due to the fact that a directly repulsive surface is accessed in the photolysis transition, the small change in the photolysis wavelength as the probe frequency is scanned is unlikely to greatly affect the fragmentation dynamics. Production of NO^+ photofragments from $(N_2O)_2^+$ and $(N_2O)_3^+$ required both photolysis (640 nm) and probe laser beams (320 nm), as the photodestruction cross-sections for $(N_2O)_n^+$ ($n = 2–3$) is negligible at 320 nm. The small time delay between the pump and probe laser pulses (< 10 ns) means that the fragment N_2O^+ rovibrational distributions should be unaffected by collisions with background gas.

Generally in the pump/probe experiments the visible photolysis laser was made sufficiently intense ($\sim 5–10$ mJ cm^{-2} pulse^{-1}) to saturate the dissociative dimer transition. On the other hand, the UV probe laser was maintained at a relatively low power level (≤ 100 μJ cm^{-2} pulse^{-1}), insufficient to saturate even the relatively strong 1_0^2 and $1_0^2 2_1^1$ transitions. In order to characterize the ion beam and to assist calibration of the fragment spectra, the $A\,^2\Sigma^+ \leftarrow X\,^2\Pi$ spectrum of the monomer N_2O^+ produced by the source was also recorded. Spectral calibration and band assignments rely on data from previous spectroscopic investigation of the N_2O^+ ion [4,12–14] with the 1_0^2 and 1_0^3 transition origins used as reference points.

3. Results and discussion

3.1. Photodestruction profiles and fragmentation branching ratios

The photodissociation cross-sections for $(N_2O)_n^+$ clusters ($n = 2–4$) between 532 and 655 nm (normalized with respect to the Ar_3^+ photodissociation cross-section [1]) are listed in Table 1. A glance at the cross-sections shows that the general form of the dimer, trimer and tetramer absorption curves are similar, with all three exhibiting a peak at ~ 600 nm (16700 cm^{-1}), although it would appear that the peak cross-sections for the trimer and tetramer are $\sim 20\%$ larger than for the dimer.

A similarity between the absorption profile of larger homogeneous cation clusters and the one of the dimer has often been interpreted as evidence that the larger cluster consist of a charged dimer core surrounded by less strongly bound neutral ligands, with the dimer core serving as the cluster chromophore in the visible and near-UV spectral regions [1]. For example, this appears to be the case for the $(N_2)_n^+$ series where the larger clusters have absorption profiles that closely resemble the one of N_4^+ [1]. On the other hand, the Ar_3^+ trimer has a distinctly different absorption profile from the dimer, and rather than having an $Ar_2^+–Ar$ minimum energy structure, seems to exist in a linear symmetric form, a view supported by calculations [1]. The available thermochemical clustering data are consistent with the larger $(N_2O)_n^+$ clusters consisting of a dimer core surrounded by less strongly bound ligands with incre-

Table 1
Photodissociation cross-sections and branching ratios for $(N_2O)_n^+$ clusters

λ (nm)	C.S. Ar_3^+ ($\mathring{A}^2$)	C.S. $(N_2O)_2^+$ ($\mathring{A}^2$)	C.S. $(N_2O)_3^+$ ($\mathring{A}^2$)	C.S. $(N_2O)_4^+$ ($\mathring{A}^2$)	$(N_2O)_3^+ \rightarrow$ dimer (%)	$(N_2O)_4^+ \rightarrow$ dimer (%)
355					0.0	0.0
405					0.0	10
532	0.76	0.33	0.34	0.35	0.0	29
546	0.68	0.27	0.51	0.49	0.0	32
575	0.48	0.51	0.85	0.88	2.7	36
607	0.28	0.94	1.10	1.10	3.3	39
630	0.17	0.71	0.94	0.95	4.0	45
640	0.13	0.61	1.00	1.00	4.0	46
655	0.10	0.30	0.34	0.44	4.0	50
1064					36	91

Photodissociation cross-sections for $(N_2O)_n^+$ clusters were normalized with respect to Ar_3^+ data (second column) estimated from fig. 2a of Ref. [1].

mental heats of association for the $(N_2O)_n^+$ series, determined in high-pressure mass spectrometry studies (provided in Table 2), falling sharply on going from the dimer to the trimer [6].

3.2. Monomer

The spectrum of the cooled N_2O^+ ions produced directly by the ion source, shown in Fig. 4a, is characterized by pronounced heads that can be readily identified as originating from either the ground vibrationless state or in the case of a small fraction, from the $\nu_2'' = 1$ level. In the 305–330 nm region the spectrum is dominated by the 1_0^2 transition, with its characteristic pair of heads separated by the $^2\Pi$ spin–orbit splitting ($A_{so} \approx -132.3$ cm^{-1}). Other prominent bands include the 1_0^3 transition lying 1323

cm^{-1} to higher energy from 1_0^2, and the $1_0^1 3_0^1$ transition lying 1088 cm^{-1} above 1_0^2. A somewhat weaker band is observed 226 cm^{-1} below 1_0^2, close to where the 3_0^1 transition should lie [12]. Also apparent in the spectrum is the $^2\Pi-^2\Delta_{5/2}$ component of the $1_0^2 2_1^1$ transition 181 cm^{-1} above 1_0^2, the other component being overlapped by the strong 1_0^2 band. The presence of the $1_0^2 2_1^1$ band indicates that the ν_2 bending

Table 2
Thermochemical data for the $(N_2O)_n^+ + N_2O \leftrightarrow (N_2O)_{n+1}^+$ association reactions

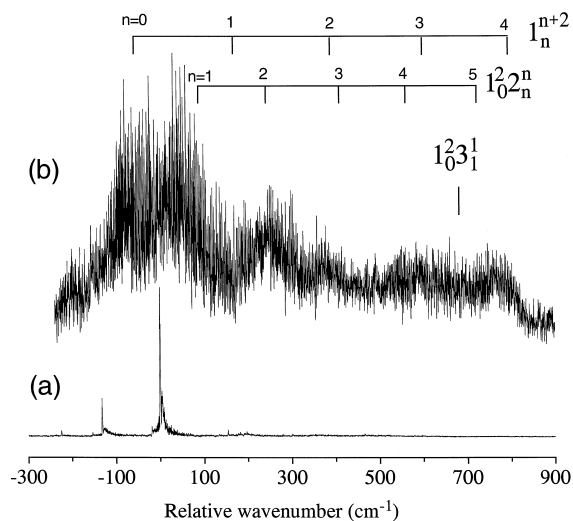| n	$-\Delta H_{n-1,n}^0$ (kcal mol^{-1})	$-\Delta S_{n-1,n}^0$ (cal mol^{-1} K^{-1})
1	17.4 ± 1.5[a]; 18.5[b]	24 ± 3[a]; 25[b]
2	5.7 ± 0.2[a]	18 ± 2[a]
3	5.6 ± 0.2[a]	24 ± 2[a]
4	4.4 ± 0.2[a]	21 ± 2[a]
5	4.1 ± 0.2[a]	22 ± 2[a]
6	~ 3.9[a]	(22)

[a] Ref. [6].   [b] Ref. [15].

Fig. 4. Predissociation spectrum of N_2O^+ ions produced: (a) directly by the ion source (best characterized by a rotational temperature of 50 K); and (b) from $(N_2O)_2^+$ photodissociation. The wavenumber scale is with respect to the $Q_{11} + P_{21}$ head of the $^2\Sigma^+ \leftarrow {}^2\Pi_{3/2}$ 1_0^2 transition. The approximate positions of sequence bands involving ν_1, ν_2 and ν_3 are marked.

mode is not completely cooled in the expansion. On the other hand, there is no sign of sequence bands involving ν_1 or ν_3, indicating that the stretching vibrations are not appreciably populated. Simulations of the 1_0^2 band demonstrate that the rotational distribution can be best characterized by a rotational temperature of 50 K, although a high-energy tail in the distribution exists.

Our analysis of the N_2O^+ photofragment spectra depends upon earlier studies of the N_2O^+ A ← X spectrum. Calloman and Creutzberg determined fundamental vibrational frequencies in both X and A states, rotational constants (B and D values) for several ground and excited state vibrational levels, and the ground state spin–orbit interaction parameter [12]. The ground $X\,^2\Pi$ and excited $A\,^2\Sigma$ states of N_2O^+ are most appropriately described as Hund's case (a) and (b), respectively, and transitions into pure stretching states have six rotational branches for each of the two spin–orbit components. Two pairs of these transitions are almost coincident leaving only four distinct branches at the level of resolution employed in our work. Two of the branches, namely P_1 and $Q_1 + P_{21}$ for the F_1 ($^2\Sigma^+ \leftarrow {}^2\Pi_{3/2}$) component and P_{12} and $Q_{12} + P_2$ for the F_2 ($^2\Sigma^+ \leftarrow {}^2\Pi_{1/2}$) component, form characteristic blue-shaded heads at $J'' \approx 30.5$–40.5 and $J'' \approx 10.5$–20.5, respectively. Several transitions terminating in higher vibronic levels of the A state (including 1_0^2, $1_0^1\,2_0^1$, 2_0^1 and 2_0^2) have been studied in fast ion beam photodissociation experiments [4]. Frey et al. [14] recorded photodissociation spectra of vibrationally excited N_2O^+ and observed several new sequence bands for ν_1. While information from earlier studies is usually sufficient to establish the vibronic identities of most of the transitions observed in the current work, there are difficulties in the rotational analysis for some of the higher vibrational levels due to a lack of the relevant rotational constants. To our knowledge, there have been no previously reported observations of the 1_0^3 transition.

3.3. Dimer

The $A\,^2\Sigma^+$–$X\,^2\Pi$ spectrum of N_2O^+ liberated in the photolysis of the $(N_2O)_2^+$ dimer at 640 nm is displayed in Fig. 4b. Surprisingly, the N_2O^+ fragment spectrum shows no sign of the band heads that are characteristic of the low-temperature N_2O^+ spectrum (Fig. 4a), proving that virtually all of the N_2O^+ fragments are formed in rotational levels with $J > 40.5$. This makes rotational analysis of the spectrum somewhat difficult, as for higher J the branches are overlapped, and the $Q_1 + P_{21}$ and $Q_{21} + R_1$ branches ($Q_{12} + P_2$ and $Q_2 + R_{12}$ for F_2 component) have almost equal spacings. An expansion of the spectrum in the region of 1_0^2 transition is shown in Fig. 5.

Altogether, more than 400 individual rotational lines have been observed for N_2O^+ photofragments from the $(N_2O)_2^+$ dimer, almost half of which can be assigned to the 1_0^2 transition using the constants of Calloman and Creutzberg [12]. The results of the assignment are conveniently displayed in the form of a Fortrat diagram (Fig. 6) where it can be seen that rotational levels with J between 45.5 and 85.5 are most significantly populated. The relative populations of rotational energy levels, obtained by dividing the rotational line intensities by the line strengths [16] and averaging over all available rotational branches and both spin–orbit components, are displayed in Fig. 7. The mean rotational energy is ~ 2000 cm^{-1} and the width of the energy distribu-

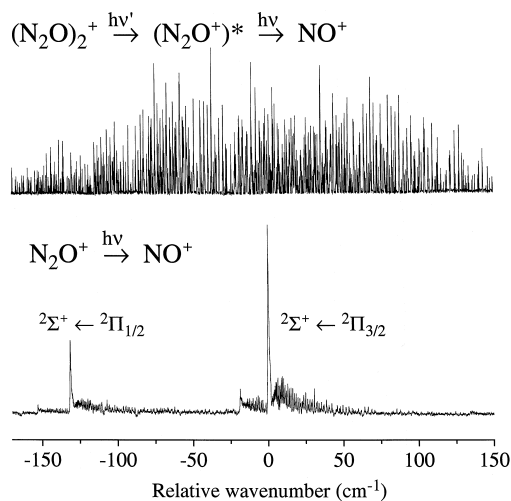Fig. 5. Spectrum of N_2O^+ ions produced from the 640 nm photolysis of $(N_2O)_2^+$ (top) compared to the spectrum of the relatively cold N_2O^+ ions formed directly in the ion source (bottom) in the region of $^2\Sigma^+ \leftarrow {}^2\Pi\ 1_0^2$ transition. The high degree of rotational excitation in the fragment N_2O^+ is evident from the absence of the low-J (~ 10.5) and intermediate-J (~ 40.5) heads.
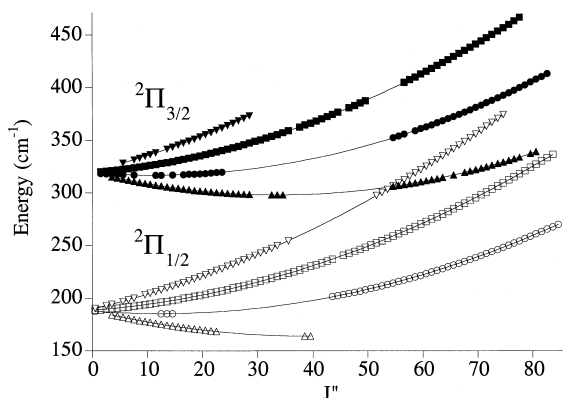
Fig. 6. Fortrat diagram for the N_2O^+ $^2\Sigma^+ \leftarrow {}^2\Pi$ transition. In the plot, low-J lines ($J \leq 50.5$) are from the spectra of N_2O^+ ions formed directly in the ion source, while high-J ones ($J \geq 40.5$) represent transitions for N_2O^+ ions from $(N_2O)_2^+$ photolysis. Triangles, circles, squares and inverted triangles denote respectively P_{1i}, $Q_{1i} + P_{2i}$, $Q_{2i} + R_{1i}$ and R_{2i} branches, where $i = 2$ (open markers, F2, $^2\Sigma^+ \leftarrow {}^2\Pi_{1/2}$ component) or $i = 1$ (filled markers, F1, $^2\Sigma^+ \leftarrow {}^2\Pi_{3/2}$ component).

tion is of the order of 1500 cm^{-1}. There does not appear to be any preference for either spin–orbit component, although fewer rotational lines could be identified for the F_2 subband. Furthermore, within experimental uncertainty, the rotational distributions for the two spin–orbit components are identical.

The bulk of the unassigned rotational lines lie to higher energy from the 1_0^2 transition and are presumably due to transitions from vibrationally excited levels (e.g., the $1_0^2 2_1^1$, $1_0^2 2_2^2$, $1_0^2 2_3^3$, 1_1^3, or $1_0^2 3_1^1$ transitions). The high fragment rotational energy and consequent absence of band heads in the spectrum means that a full rotational analysis is necessary in order for the vibrational populations to be properly determined. This does not appear to be practical at the present time due to the overlapping of branches in much of the spectrum and current limited knowledge of rotational constants for the higher vibrational levels. Given these constraints, it is merely possible to estimate that $\sim 50\%$ of the fragments are vibrationally excited by comparing the number and strength of lines assigned to the 1_0^2 transition with the unassigned lines.

If one assumes that direct dissociation from a symmetrical $(N_2O)_2^+$ complex results in N_2O and N_2O^+ fragments with identical rotational energies,

the maximum of the distribution shown in Fig. 7 corresponds to a total fragment rotational energy of ~ 4000 cm^{-1}. Given a binding energy of 6100 cm^{-1} for the complex [6], this would correspond to a maximum in the fragment translational energy distribution at ~ 0.65 eV. In contrast, translational energy distributions measured by Misev et al. between 458–660 nm indicate that the maximum at 640 nm would lie somewhat lower in energy, at ~ 0.34 eV [2]. The difference is possibly due to the fact that the measured translational energy distribution also includes contributions from fragments possessing vibrational energy that have less energy partitioned into translational motion.

3.4. Trimer

As shown in Fig. 8, the spectrum of N_2O^+ originating from the $(N_2O)_3^+$ trimer displays a rich structure, with more than 60 band heads in the $1_0^2 - 1_0^3$ region, most of which are undiscernible in the spectrum of N_2O^+ produced directly by the ion source. Particularly conspicuous in the spectrum are five broad humps, equally spaced to higher energy from the 1_0^2 band. These are most probably connected with sequence transitions involving the bending mode ν_2 (i.e., $1_0^2 2_n^n (n = 1, 2, \ldots)$), as their separations roughly corresponding to the difference in the ν_2 frequency for the A and X states (157 cm^{-1}).

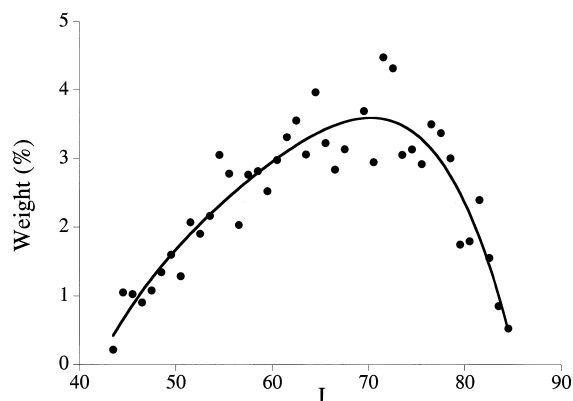Fig. 9 displays an enlarged A $\leftarrow$ X spectrum of N_2O^+ fragments from $(N_2O)_3^+$ in the 1_0^2 region,

Fig. 7. Rotational distribution of ground vibrational state N_2O^+ products from the 640 nm photodissociation of $(N_2O)_2^+$ averaged over all rotational branches of both spin–orbit components.
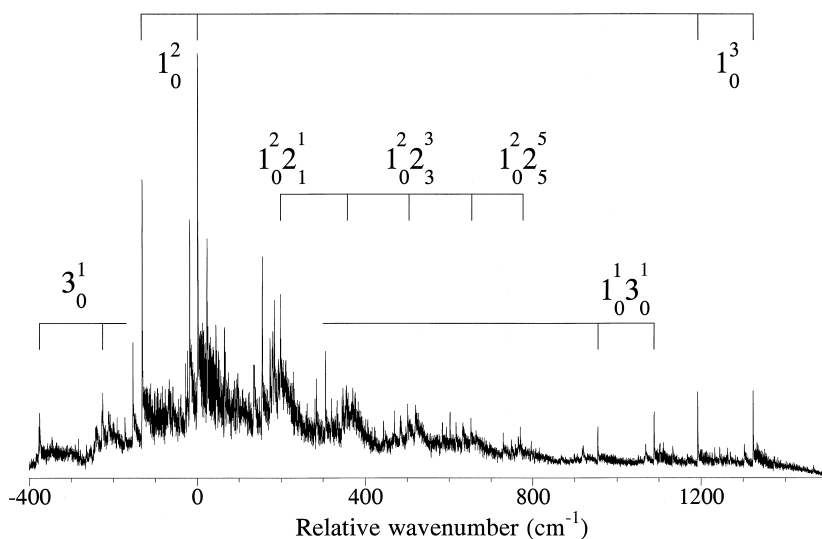
Fig. 8. Spectrum of the N_2O^+ fragments of $(N_2O)_3^+$ photodissociation near the 1_0^2 transition showing the approximate positions of sequence bands involving ν_1, ν_2 and ν_3.

where the P_1 and P_2 heads of the $^2\Pi-^2\Sigma^\pm$ components of the $1_0^2 2_1^1$ transition are clearly seen. A similar pattern is superimposed on other transitions involving upper state stretch–bend combinations (e.g., $1_0^3 2_1^1$) although because of poor S/N, usually only one or two members of the sequence could be
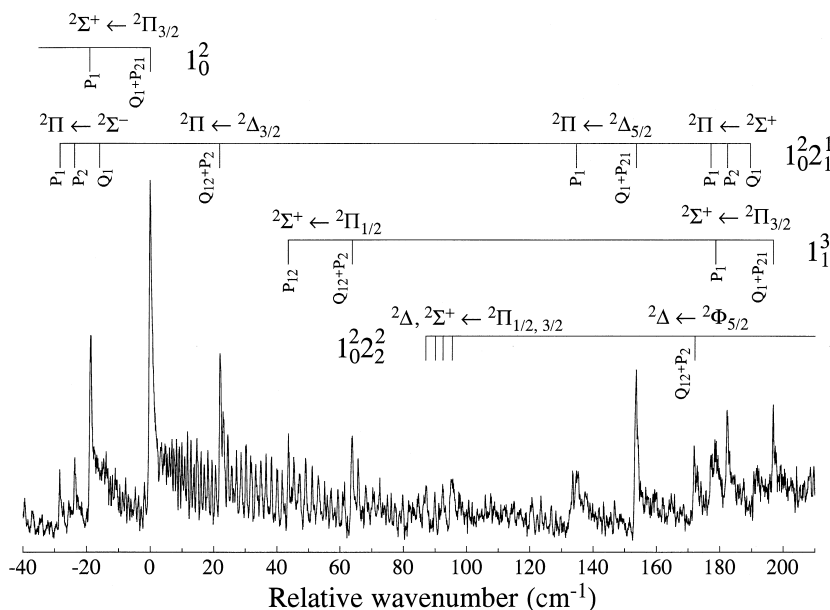

Fig. 9. Expansion of Fig. 8 near the $^2\Sigma^+ \leftarrow ^2\Pi_{3/2}$ component of the 1_0^2 transition of N_2O^+ showing vibrational assignment and rotational labels for the most prominent heads. In some cases the heads are blended with one another. For example, the Q_1 head of $^2\Pi \leftarrow ^2\Sigma^-$ Renner–Teller component of $1_0^2 2_1^1$ transition is hidden by the P_1 head of the $^2\Sigma^+ \leftarrow ^2\Pi_{3/2}$ 1_0^2 transition.

identified. A variety of other weaker transitions such as $1_0^2 2_{n+1}^n (n = 0–2)$, $1_n^{n+2} (n = 1–2)$, $1_n^{n+3} (n = 0–1)$, and $1_0^2 3_n^n$ were also observed in the 305–325 nm span. Approximately 20 of the weakest heads, possibly originating from numerous Renner–Teller components of $n\nu_2$ states with $n > 2$, were not assigned. The spectral data indicate that N_2O^+ photofragments from $(N_2O)_3^+$ can possess up to 5 quanta of ν_2 (corresponding to a vibrational energy of 2280 cm^{-1}), 2 quanta of ν_1 (vibrational energy of 2250 cm^{-1}) or 1 quantum of ν_3 (vibrational energy of 1738 cm^{-1}). A partial list of populated vibrational levels for N_2O^+ fragments from the $(N_2O)_3^+$ is provided in Table 3.

It was observed that the intensity ratio between the P_1 high-J head to that of the $Q_1 + P_{21}$ low-J head for transitions from vibrationally excited states (e.g., 1_1^3) was roughly the same as for the 1_0^2 transition, suggesting that the fragment rotational distribution is not strongly dependent on the fragment vibrational state. An estimation of the rotational excitation for N_2O^+ fragments from the trimer was obtained through analysis of the 1_0^2 transition. With the current resolution (0.3 cm^{-1}), it is impossible to measure intensities of individual lines in the spectrum as the $Q_{21} + R_1$ branch at $J \approx 23.5$ overlaps the $Q_1 + P_{21}$ branch, both of which obscure the R_{21} branch which becomes resolved only at high J values. As well, the 1_0^2 and $1_0^2 2_1^1$ transitions are partially overlapped. For this reason the 1_0^2 band profile was simulated using a Boltzmann distribution for the

rotational distribution and the line strengths provided by Earls [16]. The best fit for rotational temperature was $\sim 290 \pm 20$ K corresponding to an average rotational energy on the order of 190 cm^{-1}. The observed ratios between P_1 and $Q_1 + P_{21}$ and between P_{12} and $Q_{12} + P_2$ head intensities are satisfactorily reproduced by the simulated contour.

4. Further discussion

The photodissociation cross-section data and the N_2O^+ photofragment spectra allow us to draw certain conclusions concerning the structures and excited state dynamics of $(N_2O)_2^+$ and $(N_2O)_3^+$. As previously noted, the broad featureless absorption band of $(N_2O)_2^+$ peaking at 610 nm and extending over more than 100 nm is consistent with a transition to a directly repulsive electronic state correlating with ground state N_2O and N_2O^+ fragments [2]. As the dimer ions formed in the pulsed expansion ion source are likely to have vibrational and rotational energies that are of the same order as the monomer N_2O^+ ($T_R \approx 50$ K), it seems probable that the rotational and vibrational state of the N_2O^+ photofragments from the dimer and trimer reflect dynamical processes occurring on the excited state potential energy surface. Given the ground state geometry of the dimer ion (Fig. 1), and the fact that a directly repulsive surface is accessed, the large degree of rotational excitation ($50.5 < J < 80.5$) and excitation of the ν_2 bending vibration in the N_2O^+ fragment are not unexpected. More of a surprise, given the non-linear geometry of the ground state complex, is the activation of the ν_1 and ν_3 stretching modes. Mechanically, one would not expect that dissociation from the geometry shown in Fig. 1 would lead to a significant impulsive excitation of the two stretching vibrational modes. However even in the absence of coupling between translational and vibrational motions, excitation of these modes can result from differences in the N–N and N–O bondlengths between the dimer and the free N_2O^+ and N_2O fragments [17]. Assuming that the N–N and N–O bondlengths in the dimer lie midway between the bondlengths of the N_2O and N_2O^+ moieties, dimer photodissociation leads to a lengthening of the N–N

Table 3
Populated vibrational levels and observed transitions for N_2O^+ fragments from $(N_2O)_3^+$ photodissociation at 640 nm

Vibrational level	A state vibrational energy (cm^{-1})	Transition observed
000	0	1_0^2
010	457	$1_0^2 2_1^1$
020	914	$1_0^2 2_2^2$
030	1370	$1_0^2 2_3^3$
040	1827	$1_0^2 2_4^4$
050	2284	$1_0^2 2_5^5$
100	1126	1_1^3
200	2253	1_2^4
001	1738	$1_0^2 3_1^1$
110	1583	$1_1^3 2_1^1$

bond by 0.012 Å and shortening of the N–O bond by 0.003 Å for the N_2O^+ fragment.

One striking observation is the much lower rotational energies of N_2O^+ fragments from photodissociation of the $(N_2O)_3^+$ trimer compared to ones from the $(N_2O)_2^+$ dimer. Indeed, it appears that the N_2O^+ fragments photoejected from the trimer have only marginally higher rotational energies than N_2O^+ ions formed directly in the ion source. What is the cause of the markedly different rovibrational distributions of N_2O^+ from $(N_2O)_2^+$ and $(N_2O)_3^+$? As the dimer complex is thought to be the core for larger $(N_2O)_n^+$ clusters [6] one might expect that if the nascent N_2O^+ photofragment escapes from the cluster unimpeded, then its rovibrational distribution should be similar to the one for the dimer. The reduced rotational energy for N_2O^+ fragments from the trimer suggests that the additional N_2O ligand plays more than a spectator role in the fragmentation process. There are several scenarios that are consistent with the observations. For example, it is possible that following excitation of the dimer core, escape of the N_2O^+ fragment is blocked by the additional ligand, with a quenching of its rotational motion, possibly resulting in the formation of an energized dimer complex that subsequently undergoes decomposition. A second explanation may involve energy and charge exchange processes occurring during the breakup of the cluster, whereby the dimer core is first photolysed to produce nascent N_2O^+ and N_2O fragments both possessing rotational, vibrational and translational energy. During fission, the rapidly rotating charged fragment may undergo charge or vibrational energy exchange with the third N_2O ligand, to eventually form a rotationally quiescent N_2O^+ fragment. It is interesting to note that preliminary spectra of N_2O^+ ions photoejected from the tetramer, show that they are rotationally colder than the trimer fragments, and have a similar rotational energy distribution to the one of N_2O^+ ions issuing directly from the ion source.

Acknowledgements

References

[1] T.F. Magnera, J. Michl, Chem. Phys. Lett. 192 (1992) 99.
[2] L. Misev, A.J. Illies, F. Jarrold, T. Bowers, Chem. Phys. 95 (1985) 469.
[3] J. Lerme, S. Abed, M. Larzilliere, R.A. Holt, M. Carre, J. Chem. Phys. 84 (1986) 2167.
[4] M. Larzilliere, C. Jungen, Mol. Phys. 67 (1989) 807.
[5] R. Frey, B. Gotchev, W.B. Peatman, H. Pollak, E.W. Schlag, Chem. Phys. Lett. 54 (1978) 411.
[6] K. Hiraoka, S. Fujimaki, K. Aruga, T. Sato, S. Yamabe, J. Chem. Phys. 101 (1994) 4073.
[7] M.L. McKee, Chem. Phys. Lett. 165 (1990) 265.
[8] E.J. Bieske, J. Chem. Phys. 99 (1993) 8672.
[9] E. Bieske, J. Chem. Phys. 98 (1993) 8537.
[10] E.J. Bieske, Faraday Trans. 91 (1995) 1.
[11] N.E. Levinger, D. Ray, K.K. Murray, A.S. Mullin, C.P. Schulz, W.C. Lineberger, J. Chem. Phys. 89 (1988) 71.
[12] J.H. Callomon, F. Creutzberg, Philos. Trans. R. Soc. London 277 (1974) 157.
[13] M. Chafik el Idrissi, M. Larzilliere, J. Chem. Phys. 100 (1994) 204.
[14] R. Frey, R. Kakoschke, E.W. Schlag, Chem. Phys. Lett. 93 (1982) 227.
[15] A.J. Illies, Chem. Phys. Lett. 162 (1989) 99.
[16] L.T. Earls, Phys. Rev. 48 (1935) 423.
[17] R. Schinke, Photodissociation Dynamics, Cambridge University Press, Cambridge, 1993.